

Dynamic mesh refinement for discrete models of jet electro-hydrodynamics

Marco Lauricella^a, Giuseppe Pontrelli^a, Dario Pisignano^{b,c}, Sauro Succi^{a,*}

^a*Istituto per le Applicazioni del Calcolo CNR, Via dei Taurini 19, 00185 Rome, Italy*

^b*Dipartimento di Matematica e Fisica "Ennio De Giorgi", University of Salento, via Arnesano, 73100 Lecce, Italy*

^c*Istituto Nanoscienze-CNR, Euromediterranean Center for Nanomaterial Modelling and Technology (ECMT), via Arnesano, 73100 Lecce, Italy*

Abstract

Nowadays, several models of unidimensional fluid jets exploit discrete element methods. In some cases, as for models aiming at describing the electrospinning nanofabrication process of polymer fibers, discrete element methods suffer a non-constant resolution of the jet representation. We develop a dynamic mesh-refinement method for the numerical study of the electro-hydrodynamic behavior of charged jets using discrete element methods. To this purpose, we import ideas and techniques from the string method originally developed in the framework of free-energy landscape simulations. The mesh-refined discrete element method is demonstrated for the case of electrospinning applications.

1. Introduction

Discrete element methods are widely employed to model fluid flows in air channels, pipes and several other applications, such as modeling ink-jet printing processes, electrospinning, spray jets, micro-fluid dynamics in nozzles, etc. [1, 2, 3, 4, 5]. In particular, unidimensional jets can be easily modeled as a sequence of discrete elements by defining a mesh of points, which is used to discretize a continuous object (e.g. a liquid body) as a finite sequence of discrete elements. The aim of such model is to provide a relatively simple computational framework based on particle-like ordinary differential equations, rather than on the discretization of the partial differential equations of continuum fluids. Electro-hydrodynamic flows, however, are often subject to strong interactions leading to major deformation of the jet, hence to significant heterogeneities in the spatial distribution of the discrete particle. The latter, in turn, imply a loss of accuracy of the numerical method, since the most stretched portions of the jet become highly under-resolved. One of these cases is the electrospinning process, where a polymeric liquid jet is ejected from a nozzle and accelerated towards a conductive collector by a strong electric field. In this framework, the jet is stretched so that its diameter decreases below the micrometer-scale, providing a one-dimensional structure with very high surface area to volume ratio. This intriguing feature of the resulting polymer nanofibers spawned several papers [6, 7, 8, 9, 10, 11] and books [12, 13, 14] focussing on the electrospinning process.

In this framework, pioneering works by the Reneker and Yarin groups were focused on developing *ad-hoc* discrete element methods for electrospinning, which describe nanofibers as a series of beads obeying the equations of Newtonian mechanics [1, 15]. This modeling approach has gained an important role in predicting the outcome of electrospinning experiments. In addition, such models might support experimental researchers with a likely starting point for calibrating processes in order to save time before subsequent optimization work.

In these models, the excess charge is distributed to each element composing the jet representation, and it is static in the frame of reference of the extruded fluid jet. Once the solution surface tension is overcome by

*Corresponding author

Email address: s.succi@iac.cnr.it (Sauro Succi)

electrical forces at the spinneret, the jet serves as fluid medium to push away the mutually repulsing electric charges from the droplet pending at the nozzle of the apparatus. The main forces affecting the jet dynamics, which are accounted for in such models, include viscoelasticity, surface tension and electrostatic interactions with the external field and among excess charges in the liquid. In particular, the Coulomb repulsion between electric charges triggers bending instabilities in electrically charged jets, as demonstrated by Reneker et al. [15]. Despite being often neglected, air drag and aerodynamic effects, which may also lead to bending instabilities, have been recently modeled by discrete element methods [16, 17, 18]. Further, several complex viscoelastic models were included in order to simulate viscoelastic Boger fluid solutions [19, 20]. Systematic investigations were carried out on several simulations parameters: polymer concentration, solution density, electric potential, and perturbation frequency [21, 22].

Notwithstanding a satisfactory, though generally qualitative, agreement with experimental results has been shown [23, 24, 15], all these methods suffer the non-constant resolution of the jet representation, which usually decreases downstream. Indeed, given a uniform discretization of the initial polymeric drop pending at the nozzle, the initial step of the jet dynamics is characterized by the prevalent viscoelastic force, and it leads to a second regime, when the longitudinal stress changes under the effect of the applied electric voltage, accelerating the jet towards the collector [15]. Hence, a free-fall regime describes the later jet dynamics. Since the longitudinal viscoelastic stress along the fiber is usually larger close to the nozzle, the distance between each discrete element increases as a result of the uniformly accelerated motion, which drives the farthest elements from the spinneret. As a consequence, the jet discretization close the collector becomes rather coarse to model efficiently the filament, and the information (position, velocity, radius, stress, etc.) describing the jet is lost downstream.

A refined description of jet is necessary in every instance where a high-resolution description of physical quantities is requested, such as for bending instabilities, varicose instabilities of diameter, etc. Further, a dense mesh provides a more strict assessment of the Coulomb repulsion term, which is important to properly account the transverse force acting on the jet. Recently, refinement procedures were proposed in few works in order to avoid low resolution problems downstream [25, 26]. Nonetheless, these procedures exploit only linear interpolations, and are not able to impose a uniform mesh of jet representation, which is likely the simplest choice to model properly the entire jet, from the nozzle to the collector.

Here, we present an algorithm specifically developed to address the issue. The aim of the algorithm is to recover a finer jet representation at constant time interval, before the information describing the jet is scattered downstream, so as to preserve the jet modeling representation and make the simulation more realistic. Further, the algorithm can be used to enforce several types of mesh depending on the physical quantities under investigation, providing an adaptive description of the process.

The article is organized as follows. In Sec. 2, we summarize the 3D model for electrospinning, with the set of equations of motion (EOM) which govern the dynamics of system. In Sec. 3, we present the algorithm, with the relative step for its implementation. In Sec. 4 we report a numerical example of its application within a discrete element method for electrospinning modeling. Finally, conclusions are outlined in Sec. 5.

2. Model

In this work, we apply our algorithm to the electrospinning model implemented in JETSPIN, an open-source code specifically developed for electrospinning simulation [23], which is briefly summarized in the following text. The model is an extension of the discrete model originally introduced by Reneker et al. [15]. The main assumption of such model is that the filament can be reasonable represented by a series of n discrete elements (jet beads). Each one of this elements is a particle-like labelled by an index $i - th$. A Cartesian coordinate system is taken so that the origin is located at the nozzle, and $x - axis$ is pointing perpendicularly towards a collector where the nanofiber is deposited. The nozzle is also represented as a particle like (nozzle bead) which can moves on the plane $y - z$ (further details in the following text). Given a fluid jet starting at the nozzle and labeling $i = 0$ the nozzle bead, we obtain the set of beads indexed $i = 0, 1, \dots, n$, where n denotes the bead of the other extremity of the filament. Thus, given \vec{r}_i the position

vector of a generic $i - th$ bead, we define the mutual distance between i and $i + 1$ elements

$$l_i = |\vec{\mathbf{r}}_{i+1} - \vec{\mathbf{r}}_i|. \quad (1)$$

Here, l_i stands for the length step used for discretizing the filament. Note that the length l is typically larger than the filament radius, but smaller than the characteristic lengths of other observables of interest (e.g. jet curvature radius). Denoted m_i the mass, t the time, and $\vec{\mathbf{v}}_i$ the velocity vector of $i - th$ bead, its acceleration is given by Newton's law

$$\frac{d\vec{\mathbf{v}}_i}{dt} = \frac{\vec{\mathbf{f}}_{tot,i}}{m_i}, \quad (2)$$

where $\vec{\mathbf{f}}_{tot,i}$ is the total force acting on $i - th$ bead, given as a sum of several terms

$$\vec{\mathbf{f}}_{tot,i} = \vec{\mathbf{f}}_{el,i} + \vec{\mathbf{f}}_{c,i} + \vec{\mathbf{f}}_{ve,i} + \vec{\mathbf{f}}_{st,i}. \quad (3)$$

In last Eq, $\vec{\mathbf{f}}_{el,i}$ stands for the electric force due to the external electrical potential Φ_0 imposed between the nozzle and the collector located at distance h along verson $\vec{\mathbf{x}}$, and given as

$$\vec{\mathbf{f}}_{el,i} = q_i \frac{\Phi_0}{h} \cdot \vec{\mathbf{x}}. \quad (4)$$

Denoted q_i the charge of $i - th$ bead, the net Coulomb force $\vec{\mathbf{f}}_c$ is

$$\vec{\mathbf{f}}_{c,i} = \sum_{\substack{j=1 \\ j \neq i}}^n \frac{q_i q_j}{|\vec{\mathbf{r}}_j - \vec{\mathbf{r}}_i|^2} \cdot \vec{\mathbf{u}}_{ij} \quad (5)$$

acting on the $i - th$ bead and originated from all the other $j - th$ beads. Further, we denote $\vec{\mathbf{f}}_{st}$ the surface tension force

$$\vec{\mathbf{f}}_{st,i} = k_i \cdot \pi \left(\frac{a_i + a_{i-1}}{2} \right)^2 \alpha \cdot \vec{\mathbf{c}}_i, \quad (6)$$

acting on $i - th$ bead towards the center of the local curvature (according to $\vec{\mathbf{c}}_i$ verson) to restore the rectilinear shape of the jet, given α the surface tension coefficient, a_i the jet radius, and k_i the local curvature (measured at $i - th$ bead). Finally, $\vec{\mathbf{f}}_{ve}$ stands for the viscoelastic force

$$\vec{\mathbf{f}}_{ve,i} = -\pi a_i^2 \sigma_i \cdot \vec{\mathbf{t}}_i + \pi a_{i+1}^2 \sigma_{i+1} \cdot \vec{\mathbf{t}}_{i+1}, \quad (7)$$

pulling bead i back to $i - 1$ and towards $i + 1$, with σ the stress and $\vec{\mathbf{t}}_i$ the unit vector pointing bead i from bead $i - 1$. The polymeric jet is assumed as a viscoelastic Maxwellian liquid so that σ evolves in time following the constitutive equation:

$$\frac{d\sigma_i}{dt} = \frac{G}{l_i} \frac{dl_i}{dt} - \frac{G}{\mu} \sigma_i, \quad (8)$$

where G is the elastic modulus, and μ is the viscosity of the fluid jet.

Finally, the velocity $\vec{\mathbf{v}}_i$ satisfies the kinematic relation:

$$\frac{d\vec{\mathbf{r}}_i}{dt} = \vec{\mathbf{v}}_i. \quad (9)$$

The set of three Eqs 2, 8 and 9 governs the time evolution of system.

The nozzle bead with charge \bar{q}_0 and $x_0 = 0$ is experiencing uniform circular motion in order to model fast mechanical oscillations of the spinneret[21], where we denote A the amplitude of the perturbation and ω its frequency.

The initial simulation conditions as well as the jet insertion at the nozzle are briefly described in the following. We assume that all the electrospinning simulations start with a single jet bead, which is placed at distance l_{step} from the nozzle along the x axis. The single bead represents a jet with a cross-sectional radius a_0 , defined as the radius of the filament at the nozzle before the stretching process. The jet bead has an initial velocity v_s along the x axis which is impressed by the bulk fluid velocity in the syringe needle. Evolving in time the system, this jet bead travels up to a distance $2 \cdot l_{step}$ away from the nozzle, and a new jet bead is placed at distance l_{step} between the two previous bodies (nozzle and previous jet bead). The procedure is repeated so that we obtain a series of n beads representing the jet. Therefore, the parameter l_{step} represents the length step which is used to discretize the polymer solution filament in discrete elements, and, in other words, it is the spatial resolution imposed at the nozzle before the stretching process starts acting.

Each simulation starts with only two bodies: the nozzle bead at fixed at $x_0 = 0$ and a single bead modelling an initial jet segment of cross-sectional radius a_{init} located at distance l_{step} from the nozzle along the x axis with an initial velocity v_b along the x axis equal to the bulk fluid velocity in the nozzle. Here, l_{step} denotes the length step used to discretize the polymer solution filament in discrete elements, and, in other words, it is the spatial resolution imposed at the nozzle before the stretching process starts acting. Under the effect of the external electric field the jet bead starts to move towards the collector, and as soon as it is a distance of $2 \cdot l_{step}$ away from the nozzle, a new jet bead (third body) is placed at distance l_{step} from the nozzle along the straight line joining the two previous bodies (further details in Ref. [23]).

3. Algorithm

Given a series of discrete elements representing a liquid jet (Fig. 1), our main objective is to recover a finer representation, as soon as it has become too coarse. As example, if our aim is to investigate cross section fluctuations of the nanofiber deposited on the collector at a length scale of 1 mm, as soon as the stretching process moves two beads of the discretized jet at mutual distance larger than 1 mm, the representation is too coarse for resolving such fluctuations at the desired length scale. For this purpose, we note that the jet elements define a natural parametrization of a string (curve), which starts and ends at two given extreme points. Thus, we borrow and adapt ideas and techniques from elements of the simplified string method originally proposed by E. Weinan et al. [27] for computing the minimum energy path in an energy landscape context. In the original simplified string method, a string is dynamically evolved in the free energy landscape in order to identify the reactive path connecting two minima through a saddle point (usually the transition state of the process under investigation). An initial string is discretized by a uniform mesh (points equally spaced). Then, the string (each point of the mesh) is evolved in time by a steepest descent dynamics and the mesh undergoes the break of its uniform distribution. At constant time interval, a check on the mesh uniformity is performed, and, if necessary, the uniform representation of the mesh is reinforced by a cubic spline interpolation. Here, our idea is to apply a refinement procedure at constant time interval during the jet hydrodynamics whenever the mutual distance between any two consecutive elements representing the jet exceeds a prescribed threshold. Note that the refinement procedure should be performed before the jet representation is scattered by the stretching dynamics. In other words, we wish to preserve the modeling information before it vanishes.

By integrating in time the equations of motion above (see the field "integrate the system" in Fig 3), the observable l_i defined in Eq 1 between two consecutive elements i and $i + 1$ is found to increase under the main action of the external electric field. The algorithm proceeds in three steps as follows:

First step:

At regular interval time t_{ref} , we compute the mutual distance l_i between all the elements of the actual jet representation. Note that the parameter t_{ref} should be set in order to perform the check before the information of the jet representation is lost due to the stretching. Starting from the nozzle ($i = 0$), all the mutual distance l_i are tested for checking whether the length l_i is larger than a prescribed threshold length \tilde{l} . In particular, we mark by $s \in [0, \dots, n]$ the bead closest to the nozzle, whose distance l_s to the next bead $s + 1$ is larger than threshold \tilde{l} (see Fig 2). If $l_i < \tilde{l}$ for any i , the simulation proceeds normally, otherwise we move to the second step.

Second step:

We introduce the curvilinear coordinate $\lambda \in [0, 1]$ to parametrize the jet path, where $\lambda = 0$ identifies the nozzle, and $\lambda = 1$ the jet at the collector. For each bead we compute its respective λ_i value by using the formula:

$$\lambda_i = \frac{1}{l_{path}} \sum_{k=1}^i l_k \quad (10)$$

where $l_{path} = \sum_{k=1}^n l_k$ is the jet path length from the nozzle to the collector. In other words, we calculate the arc-lengths corresponding to the current parametrization of the string (polymer solution jet). The set of λ_i values represent the mesh used to build a cubic spline. Denoted generically by y one of the main quantities describing the jet, the data $y_i = y(\lambda_i)$ are tabulated and used in order to compute the coefficients of the spline. Note that several piecewise cubic functions are available in the literature [28]. Here, we use the Akima's algorithm [29] in order to compute spline coefficients, since it was demonstrated that other natural cubic splines could oscillate, whenever the tabulated values change quickly [28]. The cubic coefficients are computed for all the main quantities describing the jet beads (positions, fiber radius, stress, velocities)

Third step:

The filament is refined starting from the bead with index s up to the last bead (the farthest bead from the nozzle $i = n$), and only in this part of the string a uniform discretization of arc-length equal to \tilde{l} is imposed to the representation. In fact, we use a uniform discretization only for the sake of simplicity, and this choice is not mandatory. The interpolation is performed by using the spline coefficients previously computed in the *second step*. Starting from the bead with index s , we enforce the equal arc-length parametrization (uniform parametrization) of the filament by imposing all the arc-lengths of the elements to be equal to \tilde{l} (see Fig 2). First of all, we define the number of beads in the new representation as:

$$n^* = s + \left\lceil \frac{\sum_{k=s+1}^n l_k}{\tilde{l}} \right\rceil, \quad (11)$$

where the symbol $\lceil \cdot \rceil$ denotes the ceiling function. Denoted $n_{ref} = \left\lceil \frac{\sum_{k=s+1}^n l_k}{\tilde{l}} \right\rceil$, the new mesh λ_i^* is obtained as:

$$\lambda_i^* = \begin{cases} \lambda_i & \text{if } i \leq s \\ \lambda_{i-1}^* + \frac{1-\lambda_s}{n_{ref}} & \text{if } i > s \end{cases} \quad (12)$$

where λ_s is the value of the parameter λ at the bead s . Note that it is still $\lambda^* \in [0, 1]$, and the parameter λ^* has the same values from zero (the nozzle) up to the bead s . In this way, we do not apply the refinement procedure close to the nozzle, where new beads are added to the system, in order to not perturb the mechanism of bead injection (for the injection mechanism see Ref [23]). Finally, the new values $y(\lambda_i^*)$ are computed for all the λ_i^* by *spline interpolation*. The procedure is performed for y to be positions, fiber radius, stress and velocities of the jet beads in order to provide the corresponding quantities in the new mesh λ_i^* . Then, the new system is evolved in time following Eqs. 1. It is worth stressing that, in principle, it is also possible to define an adaptive mesh of the string by using a suitable weight function of a generic observable O of the string (e.g. jet radius).

A summarizing flow chart of the algorithm has been sketched in Fig 3. It is worth stressing that, notwithstanding the length of the curve in Eq 10 is computed by linear interpolation, the above procedure of reparametrization has the accuracy of a third-degree polynomial, since we use Akima's cubic spline for the interpolation of the curve. This is fine, since we care mostly about preserving the string accuracy than computing carefully its arc-length.

4. Applications on electrospinning

The dynamic refinement method was implemented in a modified version of JETSPIN, an open-source code specifically developed for electrospinning simulations [23]. The JETSPIN code delivers a discrete

element model, which bases on the model originally introduced by Reneker et al. [15]. As a test case, we perform a simulation for a polyvinylpyrrolidone (PVP) solution, which is commonly used in electrospinning experiments [10, 30]. The simulations are carried out by using the simulation parameters reported in Ref. [23], modeled on the experimental data reported by Montinaro et al. [11]. For convenience, all the simulation parameters are summarized in Tab. 1.

We now consider two different simulations (in the following *case I* and *case II*), the second incorporating the mesh-refined algorithm. The simulations were integrated in time for 0.2 second by the fourth order Runge–Kutta method with a time step equal to 10^{-8} sec, and the jet beads were inserted at a distance $l_{step} = 0.02$ cm from the nozzle. In the second simulation the dynamic refinement is applied every $t_{ref} = 0.001$ seconds. During the refinement procedure we impose all the arc-lengths \tilde{l} equal to 0.2 cm for the new parametrization. In both simulations, we distinguish two different regimes of the observables describing the electrospinning process. In the first, the observables follow an initial drift when the jet has not reached the collector yet. Then, all the observables fluctuate around a constant mean value (stationary regime) after the jet touches the collector. Here, we focus our attention on the latter regime. Given the series of n beads representing the jet, we define the observable:

$$R_i = \frac{l_{step}}{l_i} \quad (13)$$

where l_i is the mutual distance between i and $i + 1$ elements, and l_{step} the length step. We stress that $R \in (0, 1]$, and, in particular, R_0 is equal to 1 at the nozzle, since l_0 is imposed equal to the length step l_{step} , which is used to discretize the jet before stretching, and it works as a resolving power indicator of the actual jet representation at a specific point of the filament. Note that in the following, we use the notation $R(\lambda)$ instead of R_i just for the sake of simplicity, exploiting that, given a configuration, a unique value of λ is associated to each $i - th$ bead, where the observable R_i is computed. In Fig. 4 we show the mean value $\langle R(\lambda) \rangle$ computed as function of the curvilinear coordinate λ over the entire stationary regime. Here, we observe a quick decrease of $\langle R(\lambda) \rangle$ for the *case I*. For instance, the resolving power R is already 1/40 of its initial value at λ equal to 0.1, and it continues to decrease up to 1/200 of the initial R value close the collector at curvilinear coordinate $\lambda = 1$. On the other hand, the resolving power R for the *case II* is larger than 0.075 for any value of λ , showing that the algorithm is efficient in preventing too coarse discretization of the jet. Thus, we obtain the finer representation of the polymeric filament displayed in Fig. 5, where the beads belonging to the new discretization are colored in red, and the grains of the old one are in blue.

The higher resolving power R of *case II* safeguards a finer discrete representation of the jet which is a continuous object. This is particularly useful in modeling varicosity [31]. As an example, we report an electrospinning simulation of a varicose jet in order to test our refinement method in this special framework. Here, varicose jet stands for a filament with rapid fluctuations in its cross section radius. The varicosity was artificially induced by inserting at the nozzle a bead every ten beads with an extra 10% of mass, while all the other parameters are kept the same as in Tab. 1. This extra mass models a solid impurity, which triggers the varicosity along its jet path from the nozzle towards the collector. In Fig. 6 we report a short segment of the filament deposited at the collector for the two cases. Here, we note that in *case II* the mesh refinement is capable of representing the fluctuation of the cross section along the nanofiber. On the other hand, such information is completely missed in the *case I*, where the filament results at lower resolution. This highlights the utility of the dynamic refinement procedure, whenever our aim is to model nanofiber features of small length-scale.

Next, we offer few comments on the parameter \tilde{l} which defines the resolution parameter used in the spline interpolation of the string. It was observed by Yarin et al [1] that the discrete element modeling of a fiber by 0-dimensional point particles (beads) implies mathematical inconsistencies, as the discretization density increases. Indeed, the modeled fiber tends to an infinitely thin, one-dimensional continuous object, invalidating thus the discrete bead model. The repulsive Coulomb force is the term incurring in such issue, since the electrostatic force between two consecutive jet segments of length l_{step} and with their junction point at λ_p value in curvilinear coordinate is computed by the double integral

$$\vec{f}_{1 \rightarrow 2} = \frac{1}{4\pi\epsilon_0} \int_{\lambda_p - l_t}^{\lambda_p} d\lambda_1 \int_{\lambda_p}^{\lambda_p + l_t} d\lambda_2 \frac{q_l^2}{|\vec{r}(\lambda_2) - \vec{r}(\lambda_1)|^3} (\vec{r}(\lambda_2) - \vec{r}(\lambda_1)) \quad (14)$$

where $\vec{r}(\lambda)$ denotes the position vector along the string at curvilinear coordinate λ , and q_l is the linear charge density. It is easily seen that the integral diverges as the parameter \tilde{l} tends to zero. In an analytical study Yarin et al.[1] addressed this issue by arguing that charges are not distributed on the centerline of the fiber, but they lies rather on its outer shell of circular shape. Thus, the problem is recovered by accounting for the actual electrostatic form factors between two interacting circular sections of a charged filament. In this context, several analytical approximations were developed [1, 26, 25] for computing the local electric force acting between two contiguous rings representing jet elements. We recommend to use one of the mentioned analytical approximations, if really low values of \tilde{l} are employed during the dynamics refinement procedure. However, a reasonable value of \tilde{l} can be assessed in order to maintain a fine jet representation and avoiding, at the same time, mathematical inconsistencies. In particular, the Coulomb integral for the electrostatic repulsion between two interacting rings can be numerically computed and compared with Eq. 14 in order to estimate the error introduced by the centerline approximation at the given value of \tilde{l} . A conservative value of \tilde{l} larger than the length step l_{step} introduces a negligible error due to the centerline approximation. In this work, we impose a value of \tilde{l} which is an order of magnitude larger than length step l_{step} . In order to justify the last statement, we report in Fig 7 snapshots of several simulations performed with three distinct values of \tilde{l} equal to 0.2 cm, 0.4 cm, 0.8 cm, and a fourth simulation without the dynamic refinement activated at time t equal to 0.009 seconds, just 0.001 seconds before the jet touches the ground. Here, it is evident as the jet topology is substantially equivalent, confirming that possible errors introduced by our approximation for the Coulomb force of Eq 5 at our operative values of \tilde{l} are negligible.

Furthermore, it is worth to stress that a small value of \tilde{l} also implies a larger computational cost of the simulation. Indeed, the computation of the repulsive Coulomb force is a n -body problem, which scales as $\mathcal{O}(n^2)$ with n denoting the number of discrete elements. As example, we report in Tab. 2 the CPU wall-clock time of the three electrospinning simulations, with the dynamic refinement procedure and \tilde{l} equal to 0.2 cm, 0.4 cm, and 0.8 cm, previously mentioned. Along with these data, the computational cost of a simulation without dynamic refinement is also shown. For the sake of completeness, we also report in Tab. 2 the parallel efficiency η , which is defined as $\eta = T_s / (T_p * n_{proc})$ with T_s and T_p the CPU wall-clock time for the same job executed in serial and parallel mode, and n_{proc} the number of CPUs involved in the parallel run. Here, we note that the increase of effective CPU time is dependent on the average number of discrete elements n , as expected. In particular, we note that the simulation with dynamic refinement implies a higher CPU cost than a classical simulation (*case I*). In Ref. [25], Kowalewski et al. addressed the problem by using the hierarchical force calculation algorithm (treecode) for computing the Coulomb force, which complexity scales as $\mathcal{O}(n \log n)$ [32]. The fast multiple method (FMM) [33] can be also used to handle long-range interactions with a high computational efficiency, which theoretically achieves $\mathcal{O}(n)$ operation count. The treecode and FMM are the best candidate to overcome this issue, and its implementation in our dynamic refinement code will be considered in future works.

5. Conclusions

We have presented a dynamic mesh refinement method for addressing low resolution problems in discrete element models of jet hydrodynamics. In particular, we have shown by practical examples that the proposed algorithm is able to recover a finer representation by enforcing a uniform arc-length discretization of a fluid jet at constant time interval, before the information describing the modeled object is scattered downstream. Furthermore, the preserved jet representation is able to model short-range phenomena, such as varicosity, providing more realistic simulations. In this work, we have described the basic structure of the algorithm and the main steps for its implementation in discrete element models of the electrospinning process. In addition, we have discussed the effect of low values of the resolution parameter \tilde{l} on discrete element models and on the relative computational costs, so as to provide general guidelines for using the dynamics refinement procedure in electrospinning models.

In summary, the presented algorithm may be used for investigating complex short-range phenomena of unidimensional liquid jets as well as to improve the accuracy of discrete element models in representing electro-hydrodynamic processes. Several existing models might benefit of dynamic refinement in order to better support experiments, and provide useful insights for enhancing the efficiency of several processes involving jet hydrodynamics.

Acknowledgments

The research leading to these results has received funding from the European Research Council under the European Union's Seventh Framework Programme (FP/2007-2013)/ERC Grant Agreement n. 306357 ("NANO-JETS").

References

- [1] A. L. Yarin, S. Koombhongse, D. H. Reneker, Taylor cone and jetting from liquid droplets in electrospinning of nanofibers, *Journal of Applied Physics* 90 (9) (2001) 4836–4846.
- [2] J. Q. Feng, A general fluid dynamic analysis of drop ejection in drop-on-demand ink jet devices, *Journal of Imaging Science and Technology* 46 (5) (2002) 398–408.
- [3] K. Apostolou, A. Hrymak, Discrete element simulation of liquid-particle flows, *Computers & Chemical Engineering* 32 (4) (2008) 841–856.
- [4] H. Wijshoff, Structure-and fluid-dynamics in piezo inkjet printheads, University of Twente, 2008.
- [5] G. Dorr, J. Hanan, S. Adkins, A. Hewitt, C. O'Donnell, B. Noller, Spray deposition on plant surfaces: a modelling approach, *Functional Plant Biology* 35 (10) (2008) 988–996.
- [6] D. H. Reneker, I. Chun, Nanometre diameter fibres of polymer, produced by electrospinning, *Nanotechnology* 7 (3) (1996) 216–223.
- [7] D. Li, Y. Wang, Y. Xia, Electrospinning nanofibers as uniaxially aligned arrays and layer-by-layer stacked films, *Advanced Materials* 16 (4) (2004) 361–366.
- [8] C. P. Carroll, E. Zhmayer, V. Kalra, Y. L. Joo, Nanofibers from electrically driven viscoelastic jets: modeling and experiments, *Korea-Aust Rheol J* 20 (2008) 153–164.
- [9] C. Luo, S. D. Stoyanov, E. Stride, E. Pelan, M. Edirisinghe, Electrospinning versus fibre production methods: from specifics to technological convergence, *Chemical Society Reviews* 41 (13) (2012) 4708–4735.
- [10] L. Persano, A. Camposeo, C. Tekmen, D. Pisignano, Industrial upscaling of electrospinning and applications of polymer nanofibers: a review, *Macromolecular Materials and Engineering* 298 (5) (2013) 504–520.
- [11] M. Montinaro, V. Fasano, M. Moffa, A. Camposeo, L. Persano, M. Lauricella, S. Succi, D. Pisignano, Sub-ms dynamics of the instability onset of electrospinning, *Soft Matter* 11 (2015) 3424–3431.
- [12] S. Ramakrishna, K. Fujihara, W.-E. Teo, T.-C. Lim, Z. Ma, An introduction to electrospinning and nanofibers, Vol. 90, World Scientific, 2005.
- [13] D. Pisignano, *Polymer Nanofibers: Building Blocks for Nanotechnology*, Royal Society of Chemistry, 2013.
- [14] J. H. Wendorff, S. Agarwal, A. Greiner, *Electrospinning: materials, processing, and applications*, John Wiley & Sons, 2012.
- [15] D. H. Reneker, A. L. Yarin, H. Fong, S. Koombhongse, Bending instability of electrically charged liquid jets of polymer solutions in electrospinning, *Journal of Applied physics* 87 (9) (2000) 4531–4547.
- [16] M. Lauricella, D. Pisignano, S. Succi, Three-dimensional model for electrospinning processes in controlled gas counterflow, *The Journal of Physical Chemistry A*, Article ASAP doi:10.1021/acs.jpca.5b12450.
- [17] M. Lauricella, G. Pontrelli, I. Coluzza, D. Pisignano, S. Succi, Different regimes of the uniaxial elongation of electrically charged viscoelastic jets due to dissipative air drag, *Mechanics Research Communications* 69 (2015) 97–102.
- [18] M. Lauricella, G. Pontrelli, D. Pisignano, S. Succi, Nonlinear langevin model for the early-stage dynamics of electrospinning jets, *Molecular Physics* 113 (17-18) (2015) 2435–2441.
- [19] G. Pontrelli, D. Gentili, I. Coluzza, D. Pisignano, S. Succi, Effects of non-linear rheology on the electrospinning process: a model study, *Mechanics Research Communications* 61 (2014) 41–46.
- [20] C. P. Carroll, Y. L. Joo, Electrospinning of viscoelastic boger fluids: Modeling and experiments, *Physics of Fluids* 18 (5) (2006) 053102.
- [21] I. Coluzza, D. Pisignano, D. Gentili, G. Pontrelli, S. Succi, Ultrathin fibers from electrospinning experiments under driven fast-oscillating perturbations, *Physical Review Applied* 2 (5) (2014) 054011.
- [22] C. Thompson, G. Chase, A. Yarin, D. Reneker, Effects of parameters on nanofiber diameter determined from electrospinning model, *Polymer* 48 (23) (2007) 6913–6922.
- [23] M. Lauricella, G. Pontrelli, I. Coluzza, D. Pisignano, S. Succi, Jetspin: a specific-purpose open-source software for simulations of nanofiber electrospinning, *Computer Physics Communications* 197 (2015) 227–238.
- [24] C. P. Carroll, Y. L. Joo, Discretized modeling of electrically driven viscoelastic jets in the initial stage of electrospinning, *Journal of Applied Physics* 109 (9) (2011) 094315.
- [25] T. A. Kowalewski, S. Barral, T. Kowalczyk, *Modeling electrospinning of nanofibers*, Springer, 2009.

- [26] T. Kowalewski, S. NSKI, S. Barral, Experiments and modelling of electrospinning process, *Technical Sciences* 53 (4) (2005) 385–394.
- [27] E. Weinan, W. Ren, E. Vanden-Eijnden, Simplified and improved string method for computing the minimum energy paths in barrier-crossing events, *The Journal of Chemical Physics* 126 (16) (2007) 164103.
- [28] C. de Boor, *A Practical Guide to Splines*, Applied Mathematical Sciences, Springer New York, 2001.
- [29] H. Akima, A new method of interpolation and smooth curve fitting based on local procedures, *Journal of the ACM (JACM)* 17 (4) (1970) 589–602.
- [30] D. H. Reneker, A. L. Yarin, Electrospinning jets and polymer nanofibers, *Polymer* 49 (10) (2008) 2387–2425.
- [31] W. Yang, H. Duan, C. Li, W. Deng, Crossover of varicose and whipping instabilities in electrified microjets, *Physical review letters* 112 (5) (2014) 054501.
- [32] J. Barnes, P. Hut, A hierarchical $O(n \log n)$ force-calculation algorithm, *Nature* 324 (1986) 446–449.
- [33] L. Greengard, V. Rokhlin, A fast algorithm for particle simulations, *Journal of computational physics* 73 (2) (1987) 325–348.

Tables

ρ (kg/m ³)	ρ_q (C/L)	a_0 (cm)	v_s (cm/s)	α (mN/m)	μ (Pa·s)	G (Pa)	V_0 (kV)	ω (s ⁻¹)	A (cm)
840	$2.8 \cdot 10^{-7}$	$5 \cdot 10^{-3}$	0.28	21.1	2.0	$5 \cdot 10^4$	9.0	10^4	10^{-3}

Table 1: Simulation parameters for the simulations of PVP solution electrified jets. The headings used are as follows: ρ : density, ρ_q : charge density, a_0 : fiber radius at the nozzle, v_s : initial fluid velocity at the nozzle, α : surface tension, μ : viscosity, G : elastic modulus, V_0 : applied voltage bias, ω : frequency of perturbation at the nozzle, A : amplitude of perturbation at the nozzle.

Dynamic Refinement	\tilde{l} (cm)	# of beads	# of CPUs	CPU wall clock time (s)	η^*
no		150	24	8787	0.26
yes	0.8	267	24	12718	0.44
yes	0.4	509	24	24726	0.62
yes	0.2	1123	24	75793	0.80

Table 2: We report the CPU wall-clock time in seconds which is needed to run several simulations with and without dynamic refinement at different values of \tilde{l} . We report also the average number of beads used to discretize the jet. The benchmark was executed on a node of 2x12 core processors made of 2.4 GHz Intel Ivy Bridge cores. *It is worth to stress that the parallel efficiency η increases with the number of beads, since the communication latency cost plays a larger role as the simulation involves a small number of beads, and the computational work is consequently not well distributed over all the CPU cores.

Figures

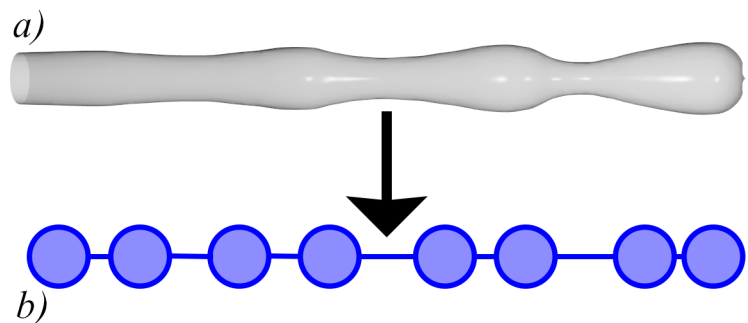


Figure 1: Sketch of a liquid jet (a) and its modeling representation by discrete elements (b) drawn as circles with connections representing the mutual interactions between two consecutive elements.

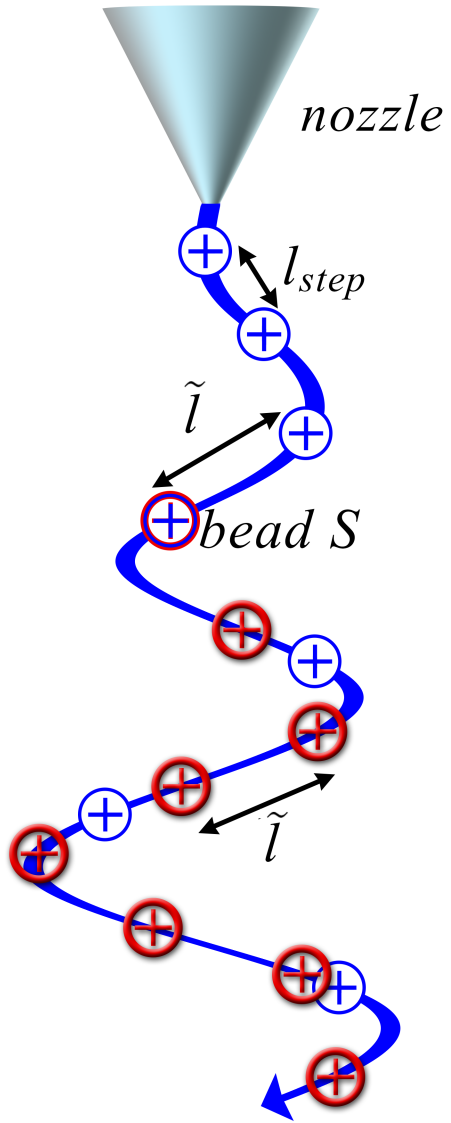


Figure 2: Diagram (not in scale) showing the actual jet representation (in blue), and the refined representation with uniform discretization of arc-length equal to \tilde{l} (in red) starting from the bead with index s . We report the length step l_{step} used to discretize the jet at the nozzle before the stretching. We also highlight the threshold distance \tilde{l} used to discern the bead where the spline interpolation starts (bead with index s). Note the string is interpolated by using a constant arc-length equal to \tilde{l} .

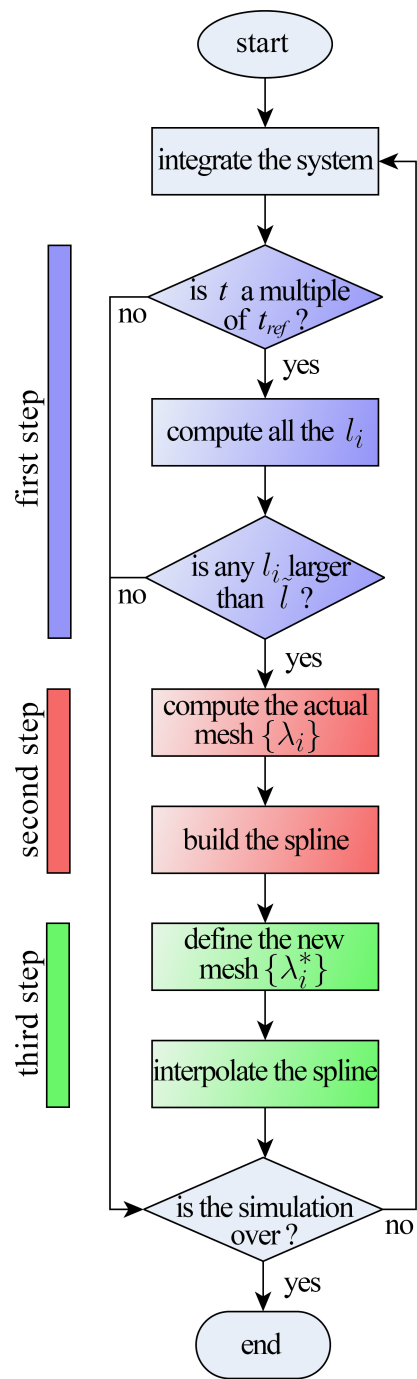


Figure 3: Flow chart of the algorithm. The three steps of the procedure are highlighted in different colors.

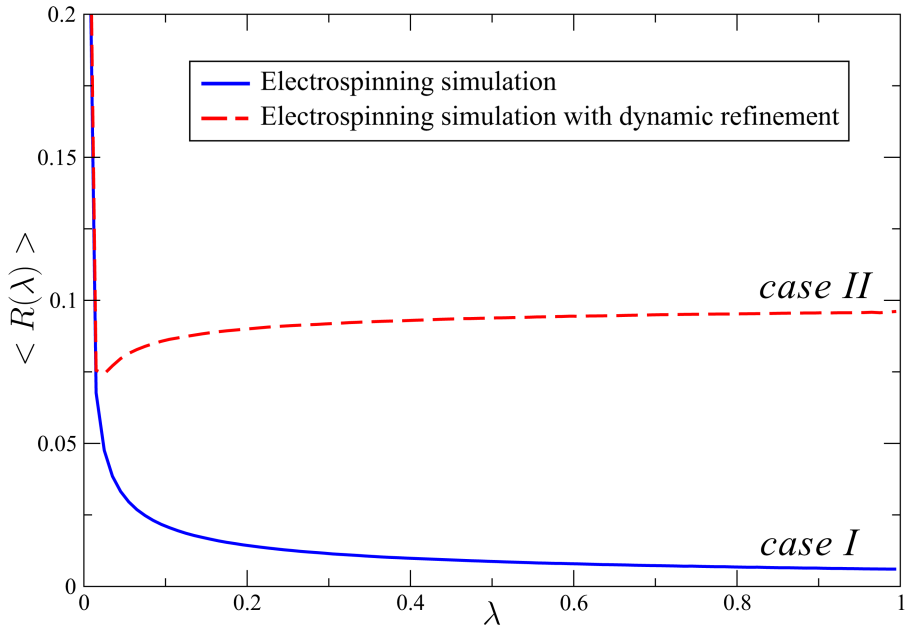


Figure 4: Mean value of the resolving power $\langle R(\lambda) \rangle$ computed as function of the curvilinear coordinate λ over the simulation time in stationary regime for the *case I* (blue line) and the *case II* (red dashed line) introduced in the text, respectively.

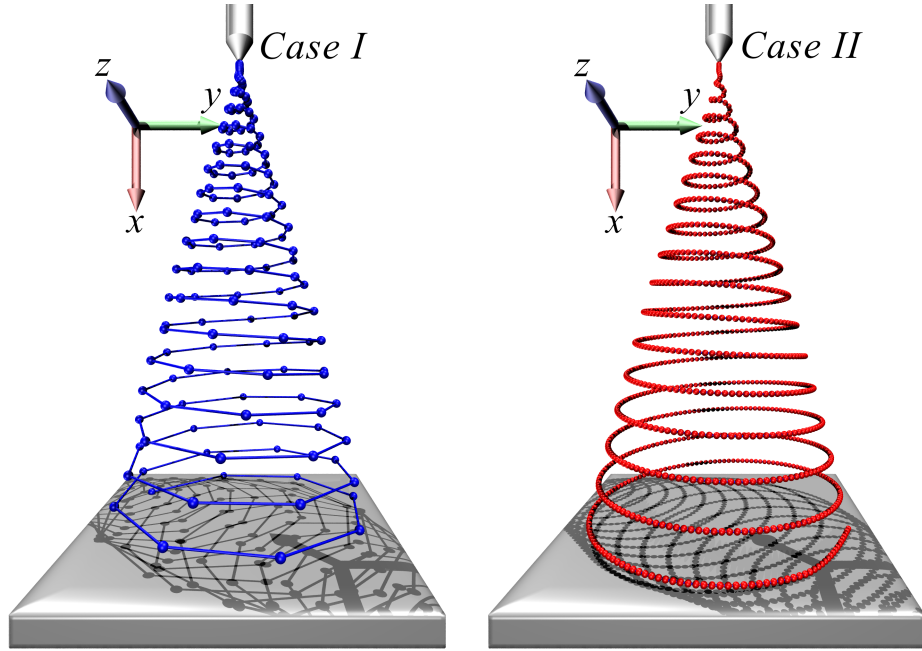


Figure 5: Two snapshots showing the jet representation in the *case I* (in blue, left panel), and in the *case II* (in red, right panel). The refined procedure was carried out in the *case II* imposing a uniform discretization with arc-length \bar{l} equal to 0.2 cm.

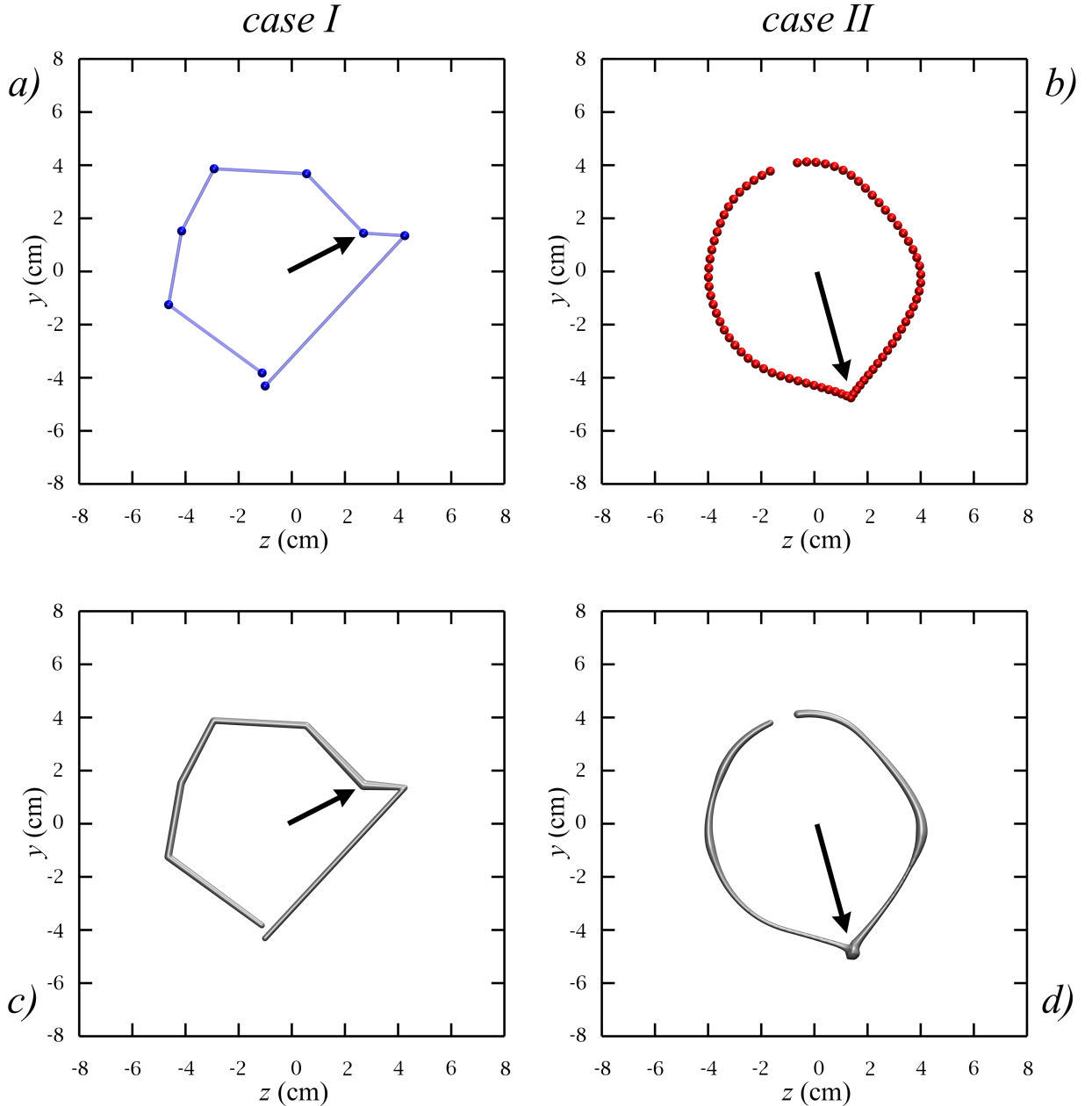


Figure 6: Snapshots of the nanofiber segments deposited on the collector for the *case I* on top left (*a*) and for the *case II* in red dashed line on top right (*b*). In black arrows we highlight varicose defects along the filaments. We also report the fiber radius profile for the *case I* on bottom left (*c*), and for the *case II* on bottom right (*d*). The cross section radius was multiplied by three orders of magnitude in order to highlight varicosity.

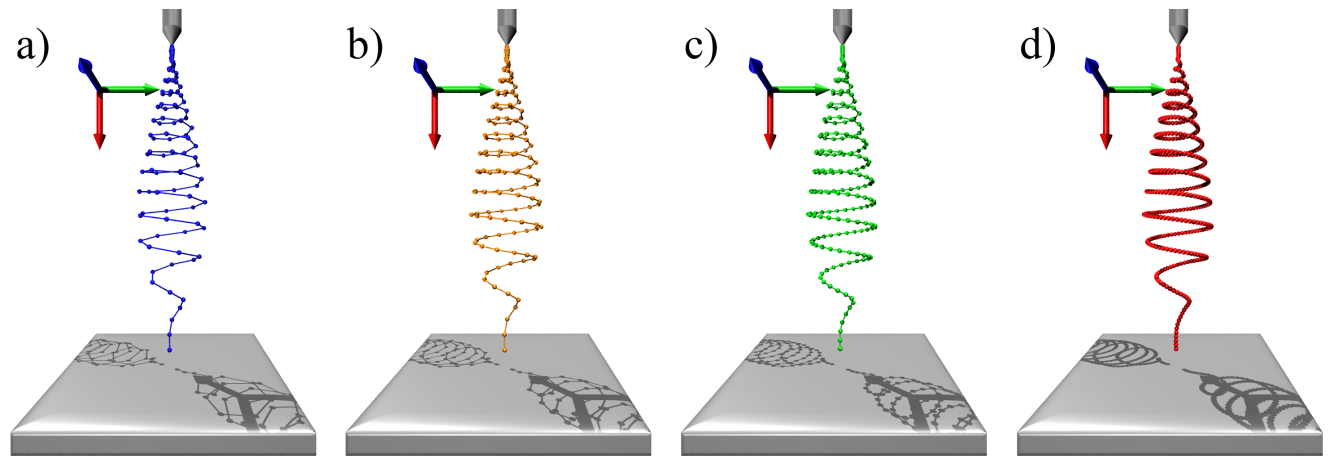


Figure 7: Snapshots of the liquid jet taken at time t equal to 0.009 seconds for four different simulations with identical simulation parameters apart the value of \bar{l} . Starting from left, denoted a) simulation without dynamic refinement activated, b), c) and d) three different simulations with dynamic refinement activated and \bar{l} equal to 0.2 cm, 0.4 cm and 0.8 cm, respectively. Note in figure we have added two lights along the bisector of the plane $y - z$ in order to emphasize the depth of field.